ADVANCED MATERIALS TECHNOLOGIES
www.advmattechnol.de

Stiff or Extensible in Seconds: Light-Induced Corrugations in Thin Polymer Sheets

*Amber M. Hubbard, Jay Kalpesh Patel, Sigurd Wagner, Chih-Hao Chang, Jan Genzer, and Michael D. Dickey**

Corrugations can dramatically change the effective mechanical properties of a thin sheet. Such alternating ridges and grooves are typically fabricated by mechanical processing. Herein, the ability to trigger and tune corrugations within thin (≈300 µm thick) thermoplastic sheets rapidly (≈seconds) using only light is reported. Patterns of black ink on the otherwise transparent, flimsy sheet preferentially adsorb external IR light, inducing localized heating of the underlying polymer. This heating causes localized shrinkage of the polymer, producing folds in the sheets; collectively, these folds result in corrugations of controlled geometry. Depending on orientation, these corrugations dramatically increase stiffness or extensibility, similar to corrugated roofs (stiff) or accordions (extensible). In the direction parallel to the folds, the maximum load-carrying capacity increases by two orders of magnitude relative to the non-corrugated sheet; perpendicular to the folds, the effective modulus decreases by four orders of magnitude. In addition to tuning effective mechanical properties, the ability to corrugate flat surfaces using light has implications for assembling 3D objects from substrates printed in 2D (such as lithographically patterned electronics) or 3D structures shipped in a flat state. Herein, the process of forming such structures is discussed and their properties are characterized.

1. Introduction

Adding geometric corrugations or cuts into materials alters the effective mechanical properties without changing the material itself.[1–8] For example, corrugated surfaces strengthen roofing materials, cardboard, and packaging without adding extra weight.[9,10] Corrugations and other spatial organization of materials can also be used to make otherwise rigid materials pliant and extensible, such as springs, accordions, and woven fabrics. This strategy has even been used at the microscale to make flexible electronics from materials that are otherwise rigid and brittle, such as silicon.[11,12]

Corrugated geometries are typically incorporated into materials during the manufacturing process, utilizing a variety of tools such as mechanical presses or thermoforming.[13,14] To circumvent the need for additional processing and to enable materials to change "on-demand," we herein present stimuli-responsive thermoplastic sheets that develop and maintain corrugations within seconds via exposure to light. Flat sheets are convenient since they are compatible with a variety of inherently 2D fabrication techniques, such as lithography or inkjet printing, and may be employed to build function (electronics, color, etc.) on the sheets before forming corrugations. Flat sheets may be efficiently transported and remotely corrugated as needed for load-bearing applications or as extensible springs, in part due to the larger length scales presented here compared with previously reported microsystems in the literature.[15–20] For example, folded microstructures can support 0.883 g, which is >7000 times the weight of the microstructures.[17] Here, we show that such principles can extend to larger structures and thus, support much larger weights.

The materials presented here undergo dramatic changes in stiffness or extensibility within seconds, using only patterning techniques (inkjet printing) combined with exposure to a commercial light bulb. This simple approach avoids complex microfabrication strategies.[1,17,18,20,21] This work is part of a broader effort in the literature to use emerging fabrication methods, such as 3D printing, to harness geometry to create materials with enhanced or unique properties. Examples include lattice structures with high strength to weight ratios[22–24] and mechanical metamaterials.[25–29]

The polymer materials reported here feature pre-strained polystyrene (PS) sheets (thickness ≈0.3 mm) that shrink by ≈55% when heated above their glass transition temperature (T_g ≈103 °C).[30–34] By only heating certain regions of the film above the T_g, it is possible to form thermal gradients on the surface that localize the shrinkage and thereby trigger a "hinging" behavior. Since the sheet is transparent, light can deliver the heat as long as there is something on the surface

Dr. A. M. Hubbard, J. K. Patel, Prof. J. Genzer, Prof. M. D. Dickey
Department of Chemical and Biomolecular Engineering
North Carolina State University
Raleigh, NC, USA
E-mail: mddickey@ncsu.edu
Prof. S. Wagner
Department of Electrical Engineering
Princeton University
Princeton, NJ, USA
Prof. C.-H. Chang
Walker Department of Mechanical Engineering
University of Texas
Austin, TX, USA
The ORCID identification number(s) for the author(s) of this article can be found under https://doi.org/10.1002/admt.202000789.

DOI: 10.1002/admt.202000789

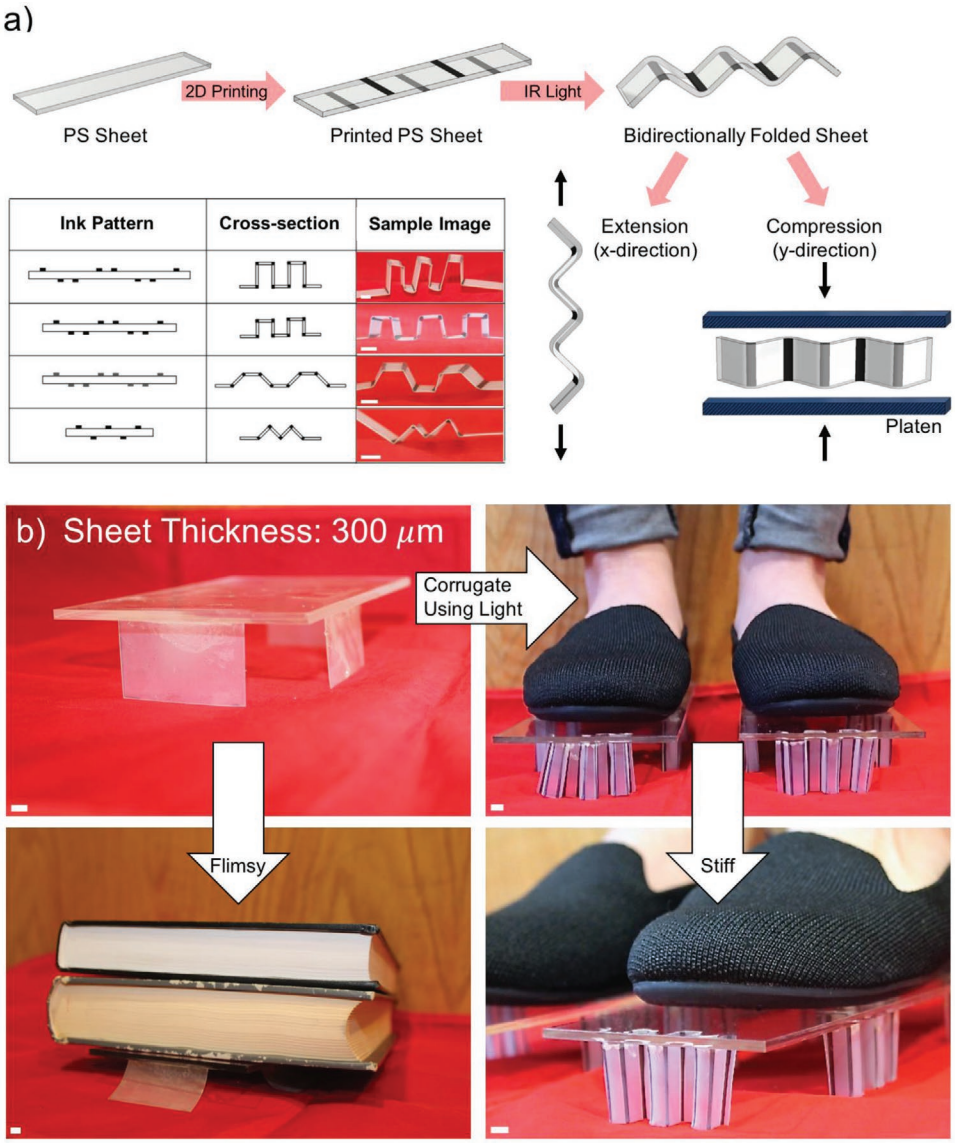

Figure 1. Corrugations induced by light can effectively render a flat sheet of plastic either extensible or stiff in seconds. a) A schematic demonstrates the sample fabrication process. Inkjet-printing patterns black ink on a 300 μm thick, pre-strained PS sheet. Upon exposure to an IR light source, the samples fold bi-directionally to form corrugated surfaces. The cross-sectional geometry and number of corrugations can be tuned based on 2D patterning of the ink. The images show samples with corrugations of rectangular, square, trapezoidal, and triangular cross-sectional geometries. b) Upper left: An acrylic platform is supported by four upright planar PS sheets. Lower left: The four planar PS sheets buckle under the weight of two books (≈1.7 kg). Right column: When loaded in the *y*-direction the four corrugated sheets support a human weighing ≈50 kg. The scale bars represent 5 mm.

to absorb it. Here, we use inkjet printing to deposit black ink onto the top and bottom surfaces of the sheets. The ink locally absorbs the light, which heats those patterned regions to generate a temperature-induced strain gradient through the thickness of the sheet, resulting in folding. By patterning ink on both the top (producing "valley" folds) and bottom (producing "mountain" folds) surfaces of the material, samples fold bidirectionally, thus producing corrugations from a planar sheet within ≈5–10 seconds. **Figure 1**a depicts a diagram of the process. Herein, we report the role of sample geometry and ink pattern on the resulting corrugations and material stiffness.

2. Results

We produced and tested four different cross-sectional geometries featuring rectangular, square, trapezoidal, and triangular profiles, as seen in Figure 1a. To explore its impact on sample extension and compression, we also varied the number of corrugations (2, 3, and 4). By corrugating the polymer sheet, the overall sample stiffness can vary, depending on the direction of compression or extension relative to the corrugations (i.e., *x*-direction or *y*-direction, in which the corrugations are always parallel with the *y*-axis, as defined in Figure 1).

To demonstrate this variable stiffness, we constructed two acrylic platforms to fix either four planar or four corrugated samples. It is important to note that the corrugated samples were initially the same size (and mass) as their planar counterparts; in other words, geometry is the only variable. We oriented the samples such that the corrugations were normal to the platform. In the case of the planar samples, two books (≈1.7 kg) placed on the acrylic platform caused the entire structure to buckle, as expected, considering the sheets are flimsy (Figure 1b). In contrast, the corrugated samples can withstand the weight of a human (≈50 kg). It should be noted that while a single platform can support the weight of a person, two were used for visualization purposes in Figure 1b; in this demonstration, the samples support >13 000 times their own weight. Alternatively, rotating the corrugated samples by 90° (such that they are compressed in the *x*-direction as defined in Figure 1), causes the corrugations to act like springs and compress in response to the weight of a smartphone (≈150 g) as seen in Figure S1a, Supporting Information.

Interestingly, the maximum load in the *x*-direction is two orders of magnitude smaller compared to the maximum load in the *y*-direction. This result is impressive because the flimsy sheets are only 300 µm thick and achieve dramatically different mechanical properties using only light to induce the geometric changes. Figure S1b and S1c, Supporting Information, show how a constant load compresses the samples significantly more in the *x*-direction compared to the same load applied in the *y*-direction.

2.1. Geometric Control

Before determining the impact of sample geometry on the resulting mechanical properties, we quantified the accuracy of the angle and precision of the folds. Figure 1a shows images of samples with both two and three corrugations (here, corrugations refers to a single "repeat unit" of a series of hinges or folds as seen in Figure S2, Supporting Information). To create hinges of consistent geometry, we used 2 mm wide patterns of ink for all hinges connecting the 5 mm long panels. All samples were 2.5 cm wide. We measured the bending angle (i.e., the angle between the adjacent PS panels) for all folds within all of the samples with a minimum of 100 measurements per geometry (cf. Figure S3, Supporting Information). The average bending angle (θ) for experimental samples with rectangular (95.2° ± 8.5°) and square (97.6° ± 7.9°) cross-sectional geometries both fall within the error of the targeted value (90°).

The average bending angle for trapezoidal samples (121.1° ± 9.5°) is also within the error of its targeted 120° bending angle despite being more difficult to manufacture than the smaller folding angles. Although the width of the inked hinge can control the folding angle,[31,35] instead we used a hinge with a constant width and controlled the angle by varying the duration of light exposure. We also used grey-scale ink (70% nominal ink density compared with black ink). The former approach involves turning the light off when reaching the desired angle. The latter approach relies on the fact that grey colored hinges absorb less light and therefore shrink less within the hinge region.

The average θ for samples with triangular cross-sections is 74.6° ± 13.2°, which is slightly higher than the expected 60° bending angle. We postulate this deviation is due to exposing the samples to the light for longer times (>10 seconds) than the samples with larger bending angles. This exposure time results in some undesired deformations. Achieving a bending angle of 60° requires extended light exposure as it requires more shrinkage in the hinged region relative to samples with 90° or 120° bending angles. The uniformity of the light illumination ultimately determines the precision of bending.

2.2. Mechanics of Samples in Compression

After production, we tested each sample mechanically to determine its stiffness (*y*-direction) and extension (*x*-direction). A plot of compressive force versus displacement can be seen in **Figure 2**a. All of the samples exhibit a characteristic behavior: after some small initial compression (the exact amount depends on the alignment of the sample with the compression platform), the load sharply increases over a small range of compressive strain. In the case of four corrugations, all corrugated samples reach a maximum load value >600 N (Figure 2a). In contrast, planar non-corrugated samples reach maximum load values <5 N (Figure S4, Supporting Information). For context, 1 N is approximately the weight of an apple. Figure 2b shows that increasing the number of corrugations from 2 to 3 increases the maximum load. Within experimental uncertainty, there is no clear increase going from 3 to 4 corrugations. Increasing the number of corrugations within a sample also increases the surface area along the edge, over which the load gets distributed. For example, for samples with square cross-sectional geometries of 2 and 4 corrugations, the surface area being compressed increases by ≈92% from 18.3 to 35.1 mm^2. Nevertheless, the similarity in the magnitude and shape of the force–displacement curves suggests that the stiffness is dictated mainly by the material and the local stress at panel joints, rather than the corrugation geometry or area.

We explain the enhancement in the maximum load for the corrugated substrates using Euler's buckling model. For a beam element compressed at the two ends, the critical force to induce buckling is given by:

$$P_{cr} = \frac{\pi^2 EI}{L} \tag{1}$$

where E is Young's modulus, I is the second moment of inertia, and L is the length of the beam element. Neglecting material changes, a corrugation in the substrate increases I, and thereby the critical force, to induce buckling failure. Letting I_o and I_{cor} be the second moments for the planar and corrugated substrates, respectively, we define a scaling relationship for the enhancement factor as:

$$\frac{I_{cor} - I_0}{I_0} \propto \frac{A^2}{t^2} \tag{2}$$

where A is the corrugation amplitude, and t is the substrate thickness (see the Supporting Information for derivation). The

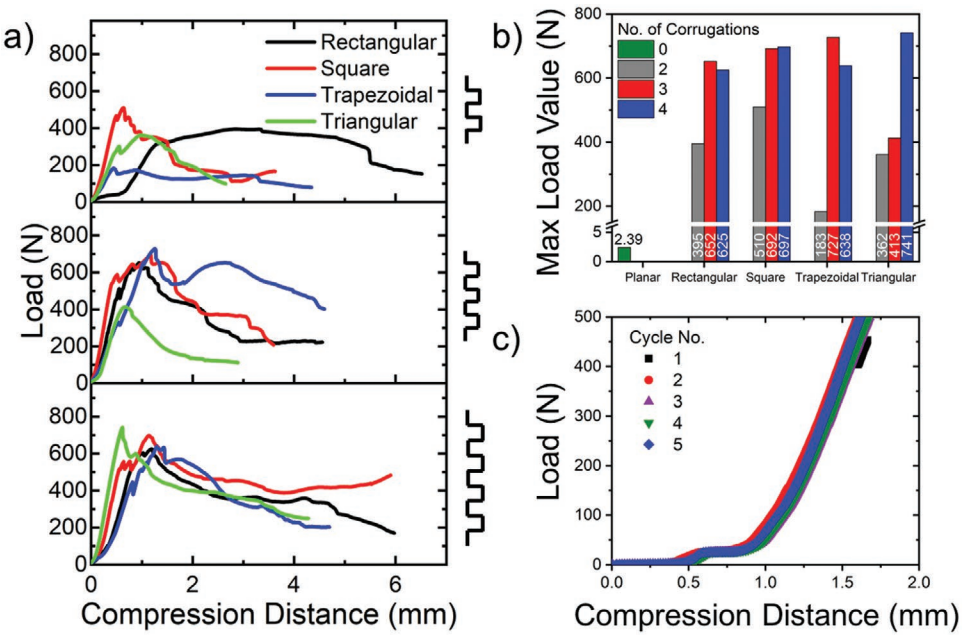

Figure 2. Corrugated samples in compression. a) Representative load–displacement curves are shown for all samples undergoing compression at a rate of 10 mm min^{-1}. b) Maximum load values for all tested samples; a minimum of four samples were tested for each design. c) A load–displacement curve for a sample with a square cross-sectional geometry and two corrugations. This cyclic compression was performed five times showing little to no hysteresis.

enhancement factor predicts how corrugations increase P_{cr} relative to a planar sheet. Increasing A increases P_{cr} necessary to cause buckling. This effect is also more dominant for thin substrates (like those used here), which tend to buckle if not corrugated. A substrate thickness of 0.3 mm and a corrugation amplitude of 4 mm raises P_{cr} by a factor of 178, which is similar in magnitude to the increase in maximum load from <5 to >600 N.

Note that this analysis examines the maximum load for failure through buckling. Given the high enhancement factor of the corrugated samples, it is likely that the structure fails as a result of exceeding critical material stresses as opposed to buckling (cf. Figure S5, Supporting Information). For a sample with two corrugations, the average stress is 27.9 MPa, which is of the same magnitude as the compressive yield strength of PS. This result indicates that given high enough corrugation amplitude, introducing the corrugated geometry can eliminate buckling failure.

We attempted to run compression tests (in the x-direction) for corrugated samples with a square cross-sectional geometry. Figure S6, Supporting Information plots a representative load–displacement trend. The maximum load values for compression tests are two orders of magnitude lower when compressed in the x-direction as compared with the y-direction. This trend is not surprising given that I does not increase in this buckling direction; in fact, maximum load values for compression in the x-direction are similar between corrugated and planar sheets. However, the corrugated samples bend far out of plane during compression, complicating the interpretation of this "spring-like" behavior.

To explore the fatigue of these corrugated sheets, we compressed a sample with two corrugations of square geometry until reaching 500 N (just below the failure point) and then recovered it. This compression cycle was performed five times with no visible cracking or failure along the sample. As seen in Figure 2c, the load–displacement curve for this test exhibits little to no hysteresis, suggesting the compression distance is not causing plastic deformation of the PS but is instead associated with the compression plates making intimate contact with the samples.

2.3. Mechanics of Samples in Extension

In addition to compression tests (y-direction), we also performed extension tests (x-direction), as seen in **Figure 3**a. We used an extensometer (Instron) to stretch samples at a strain rate of 10 mm min^{-1} until the specimens mechanically failed by breaking into two parts. All samples failed at a hinged region due to the concentration of stress at the boundary between the shrunk and unshrunk portion of the sheet. The photograph in Figure 3a reveals that the samples stretch out into almost planar sheets before breaking. In the absence of stress, the samples return back to the corrugated shape, demonstrating elastic behavior. The average angle for the hinges shown in Figure 3a demonstrates a ≈4.5% difference from the pre- and post-broken corrugated sheet; this minor difference demonstrates that the corrugations remain "elastic" even after the sheet fails by overextension.

Generally, samples with an increased number of corrugations exhibit higher extension since they have more overall length to extend (Figure 3b). Samples with rectangular cross-sections reach the highest extensions compared to the other geometries. We will discuss these extension results in detail in a subsequent section.

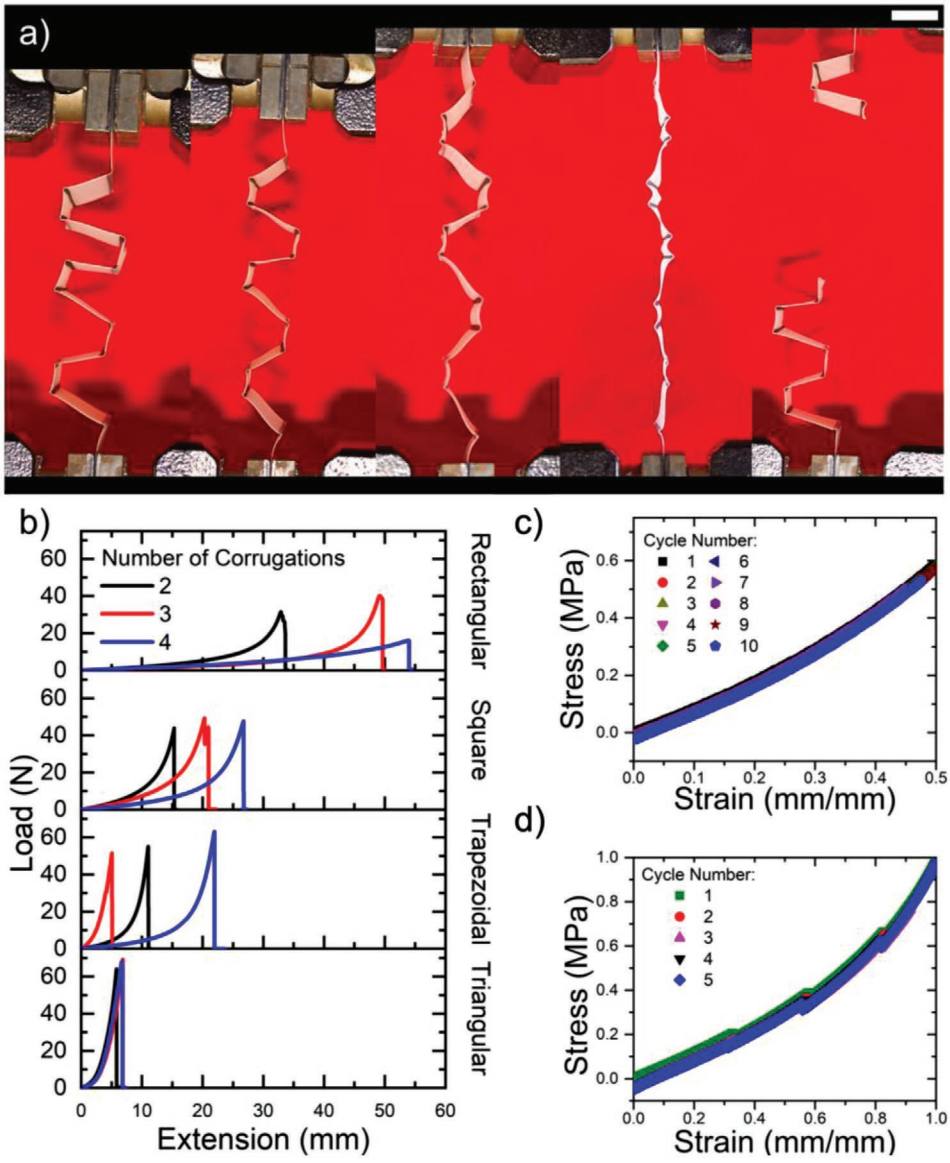

Figure 3. Corrugated samples in extension. a) A corrugated sample strained at 10 mm min^{-1} extends and flattens out until breaking. The broken portions recover elastically to the pre-extended state. The scale bar represents 5 mm. b) Representative load–displacement curves are shown for samples when extended at a strain rate of 10 mm min^{-1}. A minimum of four samples were tested for each design. c) A stress–strain curve for a rectangular sample with three corrugations cycled 10 times to a strain of 50%. d) A stress–strain curve for a rectangular sample with three corrugations cycled 5 times to a strain of 100%. No hysteresis is visible in either graph.

The corrugated samples in Figures 3c,d have an effective modulus of 0.9 ± 0.1 MPa, which is four orders of magnitude lower than that of the non-corrugated sheet (1.1 ± 0.2 GPa, Figure S7, Supporting Information). Specimens with a triangular cross-section exhibit the highest load-bearing capability during extension. This behavior is understandable considering the hinge is thicker and therefore stiffer than in the other geometries. The thickness of the hinge is due to shrinkage that occurs during IR light exposure. For example, the hinged regions account for 26% of the original sheet area in the case of triangular samples compared to 20% for the rectangular samples. Consequently, triangular and rectangular samples exhibit maximum load values of 69.2 and 40.1 N, respectively. For comparison, a planar (non-corrugated) sample of the same material exhibits a maximum load value of 256.2 ± 36.7 N. Adding corrugations to the material lowers the maximum tensile load capability (i.e., strength) in the *x*-direction while increasing extensibility and lowering the effective modulus, which we will discuss in detail below.

To further understand the extensibility of the samples in Figure 3, we performed extension tests on paper with similar corrugation patterns (cf. Figure S8 and S9, Supporting Information). We selected paper because the hinges provide little resistance to folding and unfolding since it is thinner than the PS sheets. Thus, we can compare and contrast the role of sample geometry and hinge thickness in two material systems. The

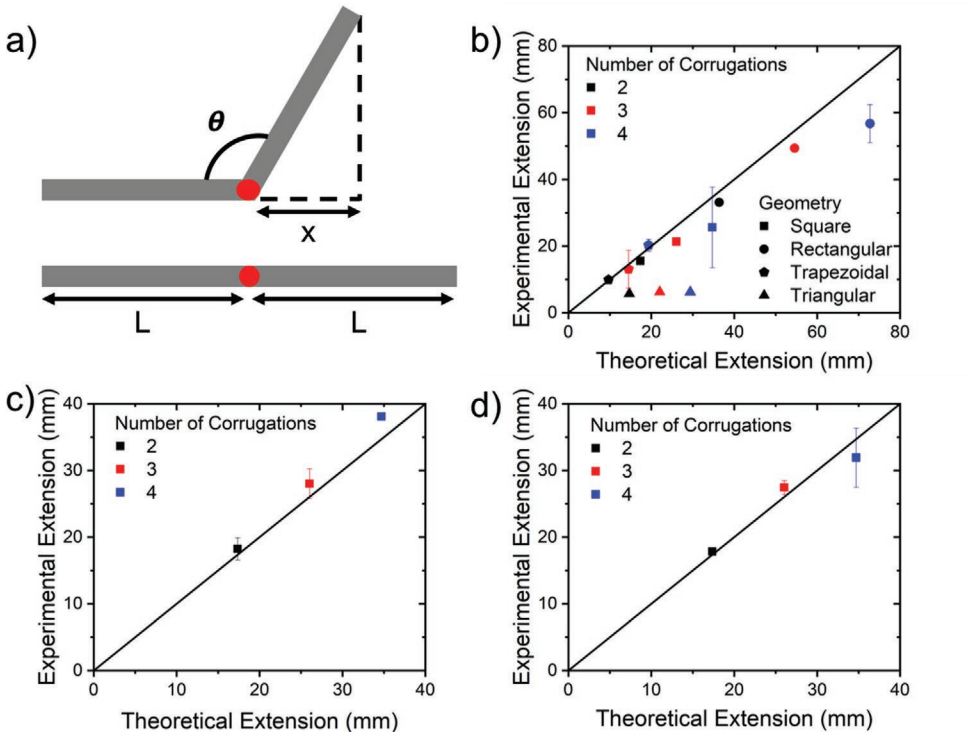

Figure 4. a) The length $L–x$ for a single fold defines the theoretical extension for a sample from a folded structure to a planar state. b) A plot of the experimental and theoretical extension values validates this simple geometric model. A diagonal line depicts a slope of one as a guide to the eye and depicts hypothetical agreement between theory and experiment. Geometry refers to the cross-sectional geometry of the corrugations. The length (L) is 5 mm for all cases except the rectangular cross-sectional geometries in which $L = 10$ mm. We plot the experimental and theoretical extension values for c) thin paper of 0.02 mm thickness and d) thick paper of 0.14 mm thickness. A minimum of three samples were tested for each design.

paper samples consisted of two thicknesses (0.02 and 0.14 mm) folded into corrugated samples with 5 mm long panels between each fold to mimic the polymer samples. During extension, paper samples with more corrugations have greater extensibility. Likewise, samples with square hinges extend further than triangular hinges, similar to the results of PS in Figure 3. Unsurprisingly, increasing the paper thickness increases the load necessary for extension (Figure S8, Supporting Information). Unless otherwise stated, all remaining reported values are for thermoplastic sheets.

We generated a simple geometric model to predict the maximum extension for each sample. **Figure 4**a shows a panel of length L with a hinge folded to θ degrees. An extensometer can extend a folded sample by length, $L–x$, back to a planar state as described in Equation 3:

$$Extension = L - x = L\left(1 - \cos\left(180^\circ - \theta\right)\right) \tag{3}$$

As seen in Figure 4b, most experimental values follow the trend predicted by Equation 3 and fall at or below the theoretical values defined by the diagonal line. We postulate the triangular samples do not follow the same trend because a higher percentage of the sample area shrinks, making it more difficult to extend the sample back to a flat state (e.g., Figure 3b); in fact, the triangular samples mechanically fail before reaching a flat state. We implement the same model for the thin (cf. Figure 4c) and thick paper samples (cf. Figure 4d). The paper samples more closely follow the theoretical trend because paper has less resistance to unfolding, which underscores the role of resistance to extension provided by the thicker hinges in the polymer samples.

To explore the elasticity and fatigue of corrugated samples, we performed cyclic tensile tests. A rectangular sample with three corrugations extended to 50% strain (cf. Figure 3c) and 100% strain (cf. Figure 3d) showed little to no hysteresis, suggesting that the corrugated sample behaves elastically and with minimal fatigue over ten cycles. The small drops in stress visible within Figure 3d originate from the hinged regions snapping into different configurations upon strain relaxation. Although we do not know the exact cause of this "snapping", it likely arises from the fact that the panels are not perfectly flat and the hinges are not always perfectly straight; thus, there may be other modes of flexure in the samples during strain. These snapping behaviors do not occur in every sample. For example, they are absent in Figure 3c.

Taken in sum, the major findings in the extensible state (i.e., in the x-direction, where deformation occurs perpendicular to the corrugations) are as follows: flat PS sheets have a modulus of ≈1–3 GPa, undergo plastic deformation during elongation, and fail at 3–5% strain with a strength of 50–100 MPa. In contrast, the corrugated structures have a modulus of ≈0.9 MPa, have elastic extensibility, and can be extended by as much as 140% strain, albeit with a relatively decreased strength of 5–10 MPa.

3. Conclusions

Introducing topography causes inextensible planar polymer sheets to undergo dramatic changes in effective mechanical behavior. These sheets possess the bulk mechanical properties of PS (a stiff, brittle, and inextensible polymer), yet become elastically stretchable or extremely stiff depending on how they are corrugated. Although the use of corrugations is an old "trick" to vary the effective mechanical performance of materials (e.g., cardboard), the novelty of this work is the use of light to induce these corrugations within seconds and, in turn, tune sample compliance and stiffness via geometric changes. After the initial exposure to light, the corrugated geometry is locked into the sheet without any additional energy input. The desired mechanical properties are achieved by altering the number of corrugations, cross-sectional geometry, and sample width.

The samples exhibit vastly different stiffness properties in the *x*- and *y*-directions. Inducing corrugations in the *y*-direction (similar to corrugated cardboard) allows for samples with a maximum compressive load up to 700 N (>14 MPa). This value is two orders of magnitude higher than the maximum compressive load of the planar, non-corrugated material (<5 N). The number of corrugations dictates the maximum load capabilities in the *y*-direction. The four corrugated sheets (300 micrometers thick) can support >50,000 g (the weight of a person) without failure.

Whereas corrugations in the *y*-direction stiffen the material, corrugations in the *x*-direction lower the effective modulus by more than three orders of magnitude from 1.1 ± 0.2 GPa to 0.9 ± 0.1 MPa. Similar to a spring, these structures allow sheets that would typically fail at 3–5% strain to extend to 140% strain. The cross-sectional geometry dictates the maximum load and extension values in the *x*-direction.

There are some limitations to this approach worth noting. 1) Though one can generate the corrugations easily, they are non-reversible. While the process presented here requires no additional energy input to maintain the enhanced mechanical properties, the ability to tune the mechanical properties in a reversible way might be desirable for certain applications. 2) Here, the sample size is limited to the irradiation area of the IR lamp (≈10 $in.^2$) used to trigger folding. Moving the lamp with respect to the sample could expose larger areas or alternative heat sources could be employed (e.g., Joule heating[36] or lasers[37]). 3) There is some notable variability in the sample bending angles, as evidenced by Figure S3, Supporting Information.

Despite the limitations, the ability to trigger significant and rapid changes to the effective mechanical properties of sheets is promising for preparing stiffness-tunable materials, creating folded devices from patterned flat surfaces (including electronics, which are patterned in 2D), and generating stiff (or compliant) structures for remote deployment using 2D sheets.

4. Materials and Methods

A pre-strained polystyrene sheet (≈0.3 mm thick), commercially known as Shrinky-Dinks, was implemented for all experiments reported here. We patterned the planar sheets with an Epson Stylus C88+ inkjet printer (black ink – Epson 60) and cut samples from the sheet using scissors. After uniform heating to 90 °C with a hot plate, a 250-Watt IR light was placed 5 cm above the sample surface and turned on. The planar samples transformed into corrugated geometries within 5–10 seconds.

We analyzed the sample's bending angles by taking images of the samples from the side and measuring the angles in ImageJ. All samples implemented 2 mm wide hinges of black ink; for samples with a trapezoidal cross-sectional geometry, we used a grey ink (70% nominal ink density). The panels between each hinge were 5 mm wide; in the case of rectangular geometries, the panels dictating height were 10 mm, resulting in a 2:1 height:width aspect ratio. For the demonstrations seen in Figure 1 and Figure S1a, Supporting Information, four samples were adhered to an acrylic platform with superglue allowing for compression in either the *x*- or *y*-direction without slippage. For the demonstrations, we employed samples with rectangular cross-sectional geometries and three corrugations. For all mechanical testing, the strain rate was 10 mm min^{-1} using an Instron (model number: 5943R7445).

Supporting Information

Supporting Information is available from the Wiley Online Library or from the author.

Acknowledgements

The authors acknowledge the National Science Foundation (NSF) Emerging Frontiers in Research and Innovation (EFRI) Program (under grant No. 1240438). The authors recognize an NSF Graduate Research Fellowship (award to A.M.H.) under Grant No. DGE-1746939 for financial support. The authors thank Professor Tori Miller for assistance with compression testing and the use of the Shimadzu compression machine; in particular, the authors thank Mr. Ben Anthony for help in operating the machine. A.M.H. thanks Mr. Mike Mantini for his insightful discussions about compression testing and Dr. Minyung Song for being a wonderful foot model who contributed to this work for the price of a coffee.

Conflict of Interest

The authors declare no conflict of interest.

Keywords

corrugation, extensibility, polymer compliance, stiffness, stimuli-responsive polymers

Received: August 9, 2020
Revised: September 24, 2020
Published online: November 20, 2020

[1] Z. Zhao, X. Kuang, J. Wu, Q. Zhang, G. H. Paulino, H. J. Qi, D. Fang, *Soft Matter* **2018**, *14*, 8051.
[2] T. C. Shyu, P. F. Damasceno, P. M. Dodd, A. Lamoureux, L. Xu, M. Shlian, M. Shtein, S. C. Glotzer, N. A. Kotov, *Nat. Mater.* **2015**, *14*, 785.
[3] J. C. Molina, J. Fiorelli, H. Savastano Jr., *Mater. Res.* **2014**, *17*, 338.

[4] W.-W. Yu, R. LaBoube, in *Cold-Formed Steel Design*, John Wiley & Sons, Ltd, New York **2010**, pp. 343–348.
[5] A. Lamoureux, K. Lee, M. Shlian, S. R. Forrest, M. Shtein, *Nat. Commun.* **2015**, *6*, 8092.
[6] Y. Xia, M. I. Friswell, E. I. S. Flores, *Int. J. Solids Struct.* **2012**, *49*, 1453.
[7] F. Côté, V. S. Deshpande, N. A. Fleck, A. G. Evans, *Int. J. Solids Struct.* **2006**, *43*, 6220.
[8] B. Liu, J. L. Silverberg, A. A. Evans, C. D. Santangelo, R. J. Lang, T. C. Hull, I. Cohen, *Nat. Phys.* **2018**, *14*, 811.
[9] S. Lou, J. C. Suhling, J. M. Considine, T. L. Laufenberg, *Mech. Cellul. Mater.* **1992**, *36*, 1.
[10] B. G. Chen, B. Liu, A. A. Evans, J. Paulose, I. Cohen, V. Vitelli, C. D. Santangelo, *Phys. Rev. Lett.* **2016**, *116*, 135501.
[11] Y. Zhang, Z. Yan, K. Nan, D. Xiao, Y. Liu, H. Luan, H. Fu, X. Wang, Q. Yang, J. Wang, W. Ren, H. Si, F. Liu, L. Yang, H. Li, J. Wang, X. Guo, H. Luo, L. Wang, Y. Huang, J. A. Rogers, *Proc. Natl. Acad. Sci. USA* **2015**, *112*, 11757.
[12] S. Xu, Z. Yan, K.-I. Jang, W. Huang, H. Fu, J. Kim, Z. Wei, M. Flavin, J. McCracken, R. Wang, A. Badea, Y. Liu, D. Xiao, G. Zhou, J. Lee, H. U. Chung, H. Cheng, W. Ren, A. Banks, X. Li, U. Paik, R. G. Nuzzo, Y. Huang, Y. Zhang, J. A. Rogers, *Science* **2015**, *347*, 154.
[13] L. Wang, Y. Yang, Y. Chen, C. Majidi, F. Iida, E. Askounis, Q. Pei, *Mater. Today* **2018**, *21*, 563.
[14] S. Li, H. Fang, S. Sadeghi, P. Bhovad, K.-W. Wang, *Adv. Mater.* **2018**, *17*, 1805282.
[15] T. Yokozeki, S. Takeda, T. Ogasawara, T. Ishikawa, *Composites, Part A* **2006**, *37*, 1578.
[16] Y. Wang, J. Weissmüller, H. L. Duan, *J. Mech. Phys. Solids* **2010**, *58*, 1552.
[17] N. Bassik, G. M. Stern, D. H. Gracias, *Appl. Phys. Lett.* **2009**, *95*, 091901.
[18] J. Breger, D. H. Shin, K. Malachowski, S. Pandey, D. H. Gracias, *MRS Adv.* **2016**, *1*, 1743.
[19] E. T. Filipov, T. Tachi, G. H. Paulino, *Proc. Natl. Acad. Sci. USA* **2015**, *112*, 12321.
[20] Z. Yan, F. Zhang, J. Wang, F. Liu, X. Guo, K. Nan, Q. Lin, M. Gao, D. Xiao, Y. Shi, Y. Qiu, H. Luan, J. H. Kim, Y. Wang, H. Luo, M. Han, Y. Huang, Y. Zhang, J. A. Rogers, *Adv. Funct. Mater.* **2016**, *26*, 2629.
[21] Z. Lin, L. S. Novelino, H. Wei, N. A. Alderete, G. H. Paulino, H. D. Espinosa, S. Krishnaswamy, *Small* **2020**, *16*, 2002229.
[22] T. A. Schaedler, A. J. Jacobsen, A. Torrents, A. E. Sorensen, J. Lian, J. R. Greer, L. Valdevit, W. B. Carter, *Science* **2011**, *334*, 962.
[23] J. Rys, L. Valdevit, T. A. Schaedler, A. J. Jacobsen, W. B. Carter, J. R. Greer, *Adv. Eng. Mater.* **2014**, *16*, 889.
[24] A. Vyatskikh, S. Delalande, A. Kudo, X. Zhang, C. M. Portela, J. R. Greer, *Nat. Commun.* **2018**, *9*, 593.
[25] B. Florijn, C. Coulais, M. van Hecke, *Soft Matter* **2016**, *12*, 8736.
[26] K. Bertoldi, V. Vitelli, J. Christensen, M. van Hecke, *Nat. Rev. Mater.* **2017**, *2*, 17066.
[27] D. Yang, L. Jin, R. V. Martinez, K. Bertoldi, G. M. Whitesides, Z. Suo, *Extreme Mech. Lett.* **2016**, *6*, 1.
[28] B. Mosadegh, P. Polygerinos, C. Keplinger, S. Wennstedt, R. F. Shepherd, U. Gupta, J. Shim, K. Bertoldi, C. J. Walsh, G. M. Whitesides, *Adv. Funct. Mater.* **2014**, *24*, 2163.
[29] T. Mullin, S. Deschanel, K. Bertoldi, M. C. Boyce, *Phys. Rev. Lett.* **2007**, *99*, 084301.
[30] Y. Liu, J. K. Boyles, J. Genzer, M. D. Dickey, *Soft Matter* **2012**, *8*, 1764.
[31] R. Mailen, Y. Liu, M. D. Dickey, M. Zikry, J. Genzer, *Soft Matter* **2015**, *11*, 7827.
[32] R. W. Mailen, M. D. Dickey, J. Genzer, M. Zikry, *J. Appl. Phys.* **2017**, *122*, 195103.
[33] R. W. Mailen, M. D. Dickey, J. Genzer, M. A. Zikry, *J. Polym. Sci. Part B: Polym. Phys.* **2017**, *55*, 1207.
[34] A. M. Hubbard, R. W. Mailen, M. A. Zikry, M. D. Dickey, J. Genzer, *Soft Matter* **2017**, *13*, 2299.
[35] Y. Liu, R. Mailen, Y. Zhu, M. D. Dickey, J. Genzer, *Phys. Rev. E* **2014**, *89*, 1.
[36] S. M. Felton, M. T. Tolley, B. Shin, C. D. Onal, E. D. Demaine, D. Rus, R. J. Wood, *Soft Matter* **2013**, *9*, 7688.
[37] Y. Liu, M. Miskiewicz, M. J. Escuti, J. Genzer, M. D. Dickey, *J. Appl. Phys.* **2014**, *115*, 1.